Hosking integral in nonhelical Hall cascade

Axel Brandenburg

Isaac Newton Institute for Mathematical Sciences, 20 Clarkson Road, Cambridge CB3 0EH, UK; and Nordita, KTH Royal Institute of Technology and Stockholm University, Hannes Alfvéns väg 12, SE-10691 Stockholm, Sweden

(23 June 2024)

The Hosking integral, which characterizes magnetic helicity fluctuations in subvolumes, is known to govern the decay of magnetically dominated turbulence. Here we show that, when the evolution of the magnetic field is controlled by the motion of electrons only, as in neutron star crusts, the decay of the magnetic field is still controlled by the Hosking integral, but now it has effectively different dimensions than in ordinary magnetohydrodynamic (MHD) turbulence. This causes the correlation length to increase with time t like $t^{4/13}$ instead of $t^{4/9}$ in MHD. The magnetic energy density decreases like $t^{-10/13}$, which is slower than in MHD, where it decays like $t^{-10/9}$. These new analytic results agree with earlier numerical simulations for the nonhelical Hall cascade.

1. Introduction

The x-ray emission from neutron stars during the first hundreds of years is believed to be powered by magnetic dissipation within their outer crusts (Gourgouliatos *et al.* 2018). Since the ions are immobile in neutron star crusts, electric currents are transported by electrons alone (Cho & Lazarian 2009). Their velocity is $\boldsymbol{u} = -\boldsymbol{J}/en_e$, where $\boldsymbol{J} = \boldsymbol{\nabla}\times\boldsymbol{B}/\mu_0$ is the current density, $\boldsymbol{B}$ is the magnetic field, e is the elementary charge, n_e is the electron density, and μ_0 is the permeability. The evolution of $\boldsymbol{B}$ is then governed by the induction equation where the electromotive force $\boldsymbol{u}\times\boldsymbol{B}$ is given by $-\boldsymbol{J}\times\boldsymbol{B}/en_e$. The induction equation therefore takes the form (Goldreich & Reisenegger 1992)

$$\frac{\partial\boldsymbol{B}}{\partial t} = \boldsymbol{\nabla}\times\left(-\frac{1}{en_e}\boldsymbol{J}\times\boldsymbol{B} - \eta\mu_0\boldsymbol{J}\right), \tag{1.1}$$

where η is the magnetic diffusivity and t is time. The $\boldsymbol{J}\times\boldsymbol{B}$ nonlinearity in this equation leads to a cascade toward smaller scales—similar to the turbulent cascade in hydrodynamics turbulence (Goldreich & Reisenegger 1992). This model is therefore referred to what is called the Hall cascade. There has been extensive work trying to quantify the amount of dissipation that occurs (Gourgouliatos *et al.* 2016, 2020; Gourgouliatos & Hollerbach 2018; Igoshev *et al.* 2021; Anzuini *et al.* 2022). Idealized simulations in Cartesian geometry resulted in power law scaling for the resistive Joule dissipation (Brandenburg 2020, hereafter B20). It depends on the typical length scale of the turbulence, the electron density, the magnetic field strength, and the presence or absence of magnetic helicity. Denoting volume averages by angle brackets, the decay of the magnetic energy density $\mathcal{E} = \langle\boldsymbol{B}^2\rangle/2\mu_0$ with time tends to follow power law behavior, $\mathcal{E}\propto t^{-p}$, where the exponent p is smaller than in magnetohydrodynamic (MHD) turbulence. Here, $\langle...\rangle$ denotes volume averaging over the spatial coordinates $\boldsymbol{x}$. In the helical case, it was found that $p = 2/5$, while for the nonhelical case, B20 reported $p\approx 0.9$. The correlation length of the turbulence, ξ, increases with time like $\xi\propto t^q$, where $q = 2/5$ in the helical case, i.e., $q = p$, and $q\approx 0.3$ in the nonhelical case. In the helical case, the exponent $2/5$ was possible to explain on dimensional grounds by

noting that the magnetic field does not correspond to a speed (the Alfvén speed, as in MHD) with dimensions $\mathrm{m\,s^{-1}}$ in SI units, but to a diffusivity with dimensions $\mathrm{m^2\,s^{-1}}$.

The decay properties of the nonhelical Hall cascade were not yet theoretically understood at the time. In the last one to two years, however, significant progress has been made in describing the decay of magnetically dominated turbulence, where a new conserved quantity has been identified, which is now called the Hosking integral (see Zhou *et al.* 2022, for details regarding the naming). The purpose of the present paper is to propose the scaling of the Hall cascade under the assumption that it is governed by the constancy of the Hosking integral, which now has different dimensions than in MHD.

2. Hosking integral and scaling for the Hall cascade

The Hosking integral $I_{\rm H}$ is defined as the *asymptotic limit of the magnetic helicity density correlation integral* $\mathcal{I}_{\rm H}(R)$ *for scales* R *large compared to the correlation length of the turbulence,* ξ, but small compared to the system size L. The original work on this integral is that by Hosking & Schekochihin (2021), who subsequently applied it to the magnetic field decay in the early universe (Hosking & Schekochihin 2022); see also Brandenburg *et al.* (2015) and Brandenburg & Kahniashvili (2017) for earlier work were inverse cascading of magnetically dominated nonhelical turbulence was first reported. The function $\mathcal{I}_{\rm H}(R)$ is given by

$$\mathcal{I}_{\rm H}(R)=\int_{V_R}\mathrm{d}^3r\,\langle h(\boldsymbol{x})h(\boldsymbol{x}+\boldsymbol{r})\rangle, \tag{2.1}$$

where V_R is the volume of a ball of radius R and $h=\boldsymbol{A}\cdot\boldsymbol{B}$ is the magnetic helicity density with $\boldsymbol{A}$ being the magnetic vector potential, so $\boldsymbol{B}=\boldsymbol{\nabla}\times\boldsymbol{A}$. We recall that $\langle...\rangle$ denotes averaging over $\boldsymbol{x}$. The function $\mathcal{I}_{\rm H}(R)$ is thus the integral over the volume $V_R=4\pi R^3/3$. For small R, it increases proportional to R^3, but for large R, it levels off. This is the value of R, which determines the Hosking integral $I_{\rm H}\equiv\mathcal{I}_{\rm H}(R)$. In practice, it is chosen empirically and must still be small compared with the size of the domain; see Hosking & Schekochihin (2021) for various examples and Zhou *et al.* (2022) for a comparison of different computational techniques for obtaining $\mathcal{I}_{\rm H}(R)$.

What matters for the Hall cascade is the fact that the dimensions of h are $[h]=[B]^2[x]$, and therefore the dimensions of $\mathcal{I}_{\rm H}$ and $I_{\rm H}$ are

$$[I_{\rm H}]=[B]^4[x]^5. \tag{2.2}$$

However, as already noted in B20, using $e=1.6\times10^{-19}\,\mathrm{A\,s}$, $\mu_0=4\pi\times10^{-7}\,\mathrm{T\,m\,A^{-1}}$, and $n_e\approx2.5\times10^{40}\,\mathrm{m^{-3}}$ for neutron star crusts, we have $en_e\mu_0\approx5\times10^{15}\,\mathrm{T\,s\,m^{-2}}$, and therefore

$$\frac{B}{en_e\mu_0}=\frac{B}{5\times10^{15}\,\mathrm{T}}\,\frac{\mathrm{m}^2}{\mathrm{s}}, \tag{2.3}$$

which is why we say B has dimensions of $\mathrm{m^2\,s^{-1}}$.† Therefore, the dimensions of $I_{\rm H}$ are

$$[I_{\rm H}]=[x]^{13}[\mathrm{s}]^{-4}. \tag{2.4}$$

Thus, given that $I_{\rm H}=$ const in the limit of small magnetic diffusivity, a self-similar evolution must imply that all relevant length scales, and in particular the magnetic

† In MHD, by comparison, the ion density ρ is a relevant quantity. Using $\rho=10^3\,\mathrm{kg\,m^{-3}}$ for solar surface plasmas, and the identity $1\,\mathrm{T}=1\,\mathrm{kg\,s^{-2}\,A^{-1}}$, we have $\mu_0=4\pi\times10^{-7}\,\mathrm{T^2\,s^2\,m\,kg^{-1}}$, and therefore $\rho\mu_0\approx3.5\times10^{-2}\,\mathrm{T\,s\,m^{-1}}$, or $B/\sqrt{\rho_0\mu_0}=(B/3.5\times10^{-2}\,\mathrm{T})\,\mathrm{m\,s^{-1}}$, which is why we say that in MHD, B has dimensions of $\mathrm{m\,s^{-1}}$.

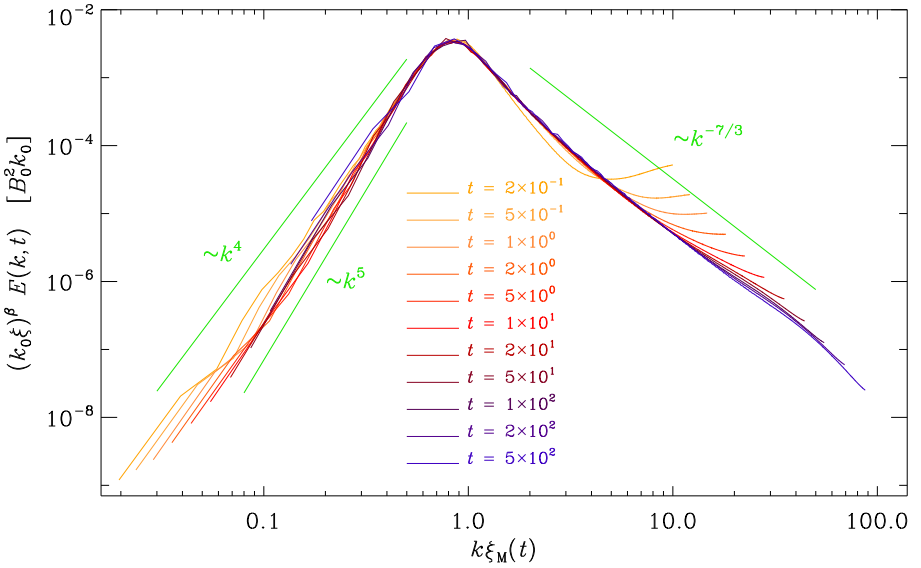

FIGURE 1. Compensated spectra for Run B of B20, which corresponds to Run B1 in the present paper. Here, $\beta = 1.7$ has been used as the best empirical fit parameter.

correlation length $\xi(t)$, must increase with time like $\xi \sim t^{4/13}$. Since $4/13 \approx 0.31$, this is indeed close to the behavior $\xi \sim t^q$ with $q \approx 0.3$ found in Sec. 3.2 of B20 (their Run B), as already highlighted in the introduction of the present paper.

To demonstrate that the energy spectra $E(k,t$ at different times are indeed self-similar, we collapse them on top of each other by plotting them versus $k\xi(t)$. Here, $\xi(t) = \mathcal{E}^{-1}\int k^{-1}E(k,t)\,\mathrm{d}k$ is the weighted integral of k^{-1}, where the spectra are normalized such that $\int E(k,t)\,\mathrm{d}k = \mathcal{E}(t)$ is the magnetic energy density. This ensures that the maxima of $E(k\xi)$ are always approximately near $k\xi(t) = 1$. In addition, we must also compensate for the decay in amplitude by multiplying the spectra by a time-dependent function, e.g., $\xi(t)^\beta$, where β is a suitable exponent, so that the compensated spectra all have the same height. In this way, we find a universal spectral function by plotting

$$[\xi(t)]^\beta\, E\big(k\xi(t),t\big) \equiv \phi\big(k\xi(t)\big). \tag{2.5}$$

As an example, we show in Figure 1 the compensated spectra for Run B of B20, which we discuss in more detail below. At this point, we just note that these were solutions to Eq. (1.1), where the initial condition consists of a nonhelical magnetic field with a spectrum $E(k) \propto k^4$ for $k \ll k_0$, with k_0 being the initial peak wavenumber. For $k \gg k_0$, we assume a decaying spectrum, here with $E(k) \propto k^{-5/3}$, although this particular choice of the exponent was not important. After some time, the spectral slopes of both subranges change: At small k, the spectrum steepens from k^4 to k^5. Beyond the peak, it falls off with a $k^{-7/3}$ inertial range, as was already found by Biskamp *et al.* (1996).

To determine the theoretically expected value of β, we invoke the condition that the compensated spectra be invariant under rescaling, $t \to \tau t'$, $\boldsymbol{x} \to \tau^q \boldsymbol{x}'$, where τ is an arbitrary scaling factor. We recall that the dimensions of $E(k,t)$ are $[x]^5[t]^{-2}$, so rescaling yields a factor τ^{5q-2}. In addition, expressing E' in terms of its universal spectral function $\phi(k\xi)$, the factor ξ^β on the left-hand side of the Eq. (2.5) produces a factor $\xi^{-\beta}$ on the right-hand side of Eq. (2.5), and therefore, after rescaling, a $\tau^{-\beta q}$ factor, i.e.,

$$E(k) \to \tau^{5q-2}\, E'(k) \propto \xi(t)^{-\beta}\tau^{-\beta q}\phi(k\xi). \tag{2.6}$$

Run	Lu	$t_1/[t]$	$t_2/[t]$	$\tilde{\eta}$	$\tilde{B}_{\rm rms}$	$\tilde{\epsilon}$	p	q	β	$p_{\rm H}$
B1	650	0.2	500	0.024	600	3×10^6	0.8 ± 0.1	0.3 ± 0.1	1.7 ± 0.1	0.16
B2	1300	3	200	0.011	700	6×10^6	0.78 ± 0.05	0.31 ± 0.05	1.6 ± 0.05	0.11

TABLE 1. Summary of runs discussed in this paper.

Therefore, $5q-2=-\beta q$ must be satisfied in order that the compensated spectra remain invariant under rescaling. Thus, $\beta=2/q-5$, as already found in B20. Inserting now $q=4/13$ yields $\beta=3/2$. The total magnetic energy density is therefore

$$\mathcal{E}=\int\xi^{-\beta}\phi(k\xi)\,{\rm d}k=\xi^{-(\beta+1)}\int\phi(k\xi)\,{\rm d}(k\xi)\propto t^{-(\beta+1)\,q}, \tag{2.7}$$

and since $\mathcal{E}\propto t^{-p}$, we have† $p=(\beta+1)\,q$. Using $\beta=2/q-5$, we have $p=2\,(1-2q)$; see Eq. (28) of B20. For $q=4/13\approx0.31$, we have $p=2\,(1-8/13)=10/13\approx0.78$, which is not quite as close to the value reported in B20 as that of q, but this could be ascribed to the lack of scale separation and also the magnetic field no longer being strong enough so that the Lundquist number,‡

$$\mathrm{Lu}=B_{\rm rms}/en_e\mu_0\eta, \tag{2.8}$$

is no longer in the asymptotic regime. This also resulted in the empirical value of β being slightly larger than the theoretical one, as we will see next.

3. Comparison with simulations for different diffusivities

In B20, various simulations of the Hall cascade have been presented, including forced and decaying simulations, helical and nonhelical ones, with constant and time-varying magnetic diffusivities, with and without stratification, etc. The main purpose of that work was to understand the dissipative losses that would lead to resistive heating in the crust of a neutron star. One of those simulations is particularly relevant for the present paper: his Run B, which had a relatively strong initial magnetic field, no helicity, large scale-separation, and a magnetic diffusivity that decreased with time in a power law fashion, allowing the simulation to retain a higher Lundquist number as the magnetic field decreases.

In the present paper, we analyze his Run B, which is here called Run B1. It is actually a new run, because we now have calculated the Hosking integral during run time. We also compare with another run (Run B2), where we decreased the magnetic diffusivity by a factor of two. As in B20, η is assumed to decrease with time proportional to $t^{-3/7}$. We kept, however, the same resolution of 1024^3 mesh points for both runs, but we must keep in mind that this can lead to artifacts resulting from a poorly resolved diffusive subrange for Run B2.

In Table 1, we compare several characteristic parameters: the start and end times,

† An equivalent, but conceptually simpler route to the $t^{-10/13}$ decay law, suggested by David Hosking (private communication), is to use Eq. (1.1) to argue that the timescale $t_{\rm dec}$ for magnetic decay is proportional to ξ^2/B. Since $t_{\rm dec}$ is proportional to t for selfsimilar decay, we get, using $\xi^5B^4=[B^2(\xi^2/B)^{10/13}]^{13/4}=(B^2t^{10/13})^{13/4}=$ const, the scaling $B^2\propto t^{-10/13}$. The difference between MHD and Hall cascade is that, in the former, $t_{\rm dec}$ is proportional to ξ/B, but $\propto\xi^2/B$ in the latter.

‡ Note that, unlike the case of MHD, in the present case of Hall cascade, no wavenumber factor enters in the definition of the Lundquist number.

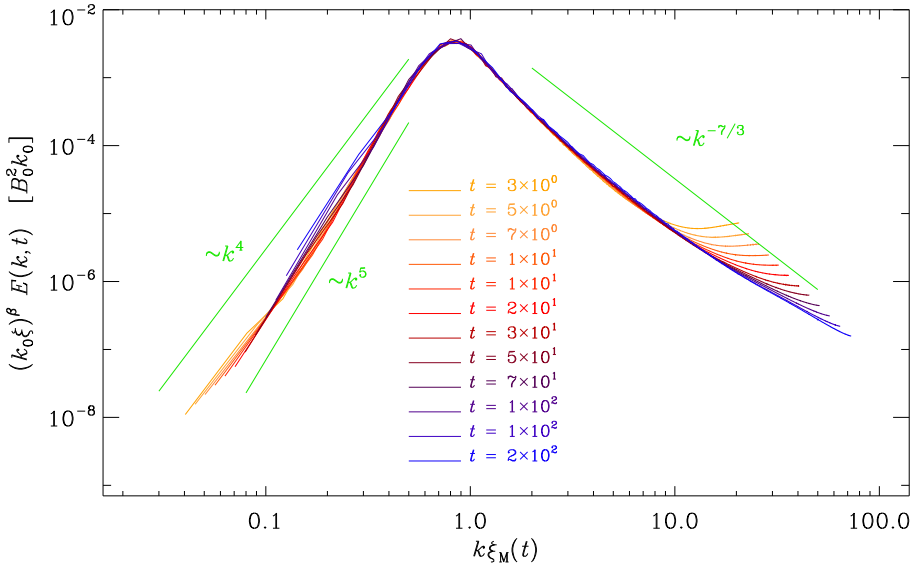

FIGURE 2. Compensated spectra for Run B2.

t_1 and t_2, respectively, of the interval for which averaged data have been accumulated, nondimensional measures of the magnetic diffusivity, the magnetic field strength, and the dissipation, $\tilde{\eta}$, $\tilde{B}_{\rm rms}$, and $\tilde{\epsilon}$, respectively, and the instantaneous scaling exponents p, q, and β. For $\tilde{\eta}$, $\tilde{B}_{\rm rms}$, and $\tilde{\epsilon}$, we compute the following time-averaged ratios:

$$\tilde{\eta} \equiv \langle t\eta/\xi^2\rangle_t, \quad \tilde{B}_{\rm rms} \equiv \langle B_{\rm rms}/(en_e\mu_0\eta)\rangle_t, \quad \text{and} \quad \tilde{\epsilon} \equiv \langle \epsilon/(e^2n_e^2\mu_0\eta^3/\xi^2)\rangle_t, \tag{3.1}$$

where $\xi(t) = \mathcal{E}^{-1}\int k^{-1}E(k,t)\,{\rm d}k$ is the correlation length and $\epsilon = \eta\mu_0\langle \boldsymbol{J}^2\rangle$ is the magnetic dissipation with $\eta = \eta(t)$, as noted above. These were also computed in B20. Time is given in diffusive units, $[t] = (\eta k_0^2)^{-1}$. In the runs of series B of B20, the value of k_0 is 180 times larger than the lowest wavenumber $k_1 \equiv 2\pi/L$ of our cubic domain of size L^3.

It turns out that a lower resistivity is important for obtaining the expected scaling. We therefore now consider Run B2, where Lu ≈ 1300. The result is shown in Figure 2, where we used $\beta = 1.6$ as the best fit, which is still slightly larger than the expected value of $3/2$, but it goes in the right direction. Therefore, we show in Figure 2 the resulting compensated spectra for Run B2, where the magnetic diffusivity is half that of Run B1 and Lu is now twice as large a before; see Table 1. We use the PENCIL CODE (Pencil Code Collaboration *et al.* 2021) and, in both cases, we use a resolution of 1024^3 mesh points.

Another comparison between Runs B1 and B2 is shown in Figure 3, where we compare their evolution in the pq–diagram. While Run B1 clearly evolves along the $\beta \approx 1.7$ line, Run B2 tends to be closer to the $\beta \approx 3/2$ line. Note also that both runs settle near the $p = 2(1-2q)$ self-similarity line (B20), although we begin to see departures near the end of the run, which is due to the finite size of the domain.

Finally, we show in Figure 4 the scalings of $I_{\rm H}(t)$, where we see that the decay exponent $p_{\rm H} \equiv -{\rm d}\ln I_{\rm H}/{\rm d}\ln t$ is about $p_{\rm H} \approx 0.16$ for Run B1 and about 0.11 for Run B2. Earlier work by Zhou *et al.* (2022) showed that $p_{\rm H}$ decreases as the Lundquist number increases, and is, in MHD, around 0.2 for Lu $\approx 10^3$, and decreases to $p_{\rm H} \approx 0.01$ for Lu $\approx 4\times10^7$. Such large values can currently only be obtained with magnetic hyper-diffusivity (Hosking

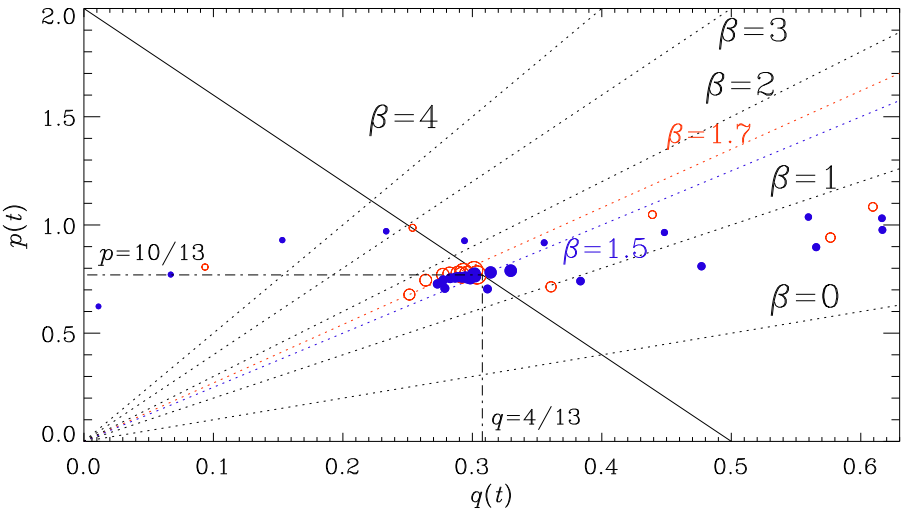

FIGURE 3. pq diagrams for Runs B1 (open red symbols) and B2 (closed blue symbols). Larger symbols denote later times.

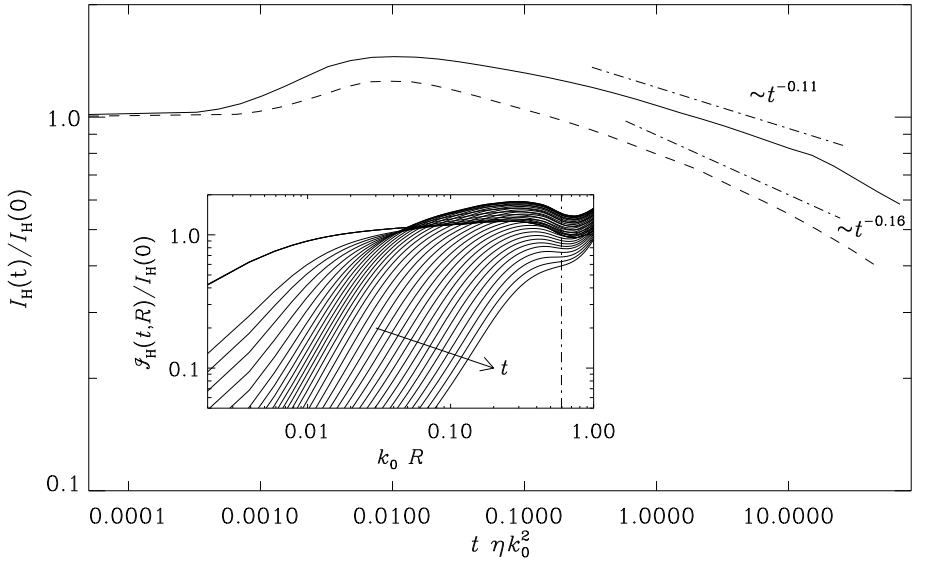

FIGURE 4. Evolution of $I_{\rm H}(t)$, showing first a slight increase and then a decline proportional to $t^{-0.16}$ for Run B1 and proportional to $t^{-0.11}$ for Run B2. The inset shows the evolution of $\mathcal{I}_{\rm H}(R;t)$ as a function of R for increasing values of t (indicated by the arrow) for Run B2. The abscissae of the main plot and the inset are normalized by ηk_0^2 and k_0, respectively.

& Schekochihin 2021; Zhou *et al.* 2022), but this has not been attempted in the present work.

As already noted by Zhou *et al.* (2022), there is an initial increase in $I_{\rm H}(t)$. This is explained by the fact that the magnetic field obeys Gaussian statistics initially, but not during the later evolution. The inset shows the R dependence of $\mathcal{I}_{\rm H}(R;t)$ for different t. The relevant value of R is deemed to be at the location where the local slope of $\mathcal{I}_{\rm H}(R)$ is minimum at late times.

MHD	$[B]=[x]/[t]$	$[\langle h\rangle]=[x]^3/[t]^2$	$q=2/3$ (helical)
		$[I_{\rm H}]=[x]^9/[t]^4$	$q=4/9$ (nonhel)
	$[E(k,t)]=[x^3][t]^{-2}$	$\beta=2/q-3$	$\beta=2\cdot 9/4-3=3/2$
		$p=2\,(1-q)$	$p=2\,(1-4/9)=10/9$
Hall	$[B]=[x]^2/[t]$	$[\langle h\rangle]=[x]^5/[t]^2$	$q=2/5$ (helical)
		$[I_{\rm H}]=[x]^{13}/[t]^4$	$q=4/13$ (nonhel)
	$[E(k,t)]=[x^5][t]^{-2}$	$\beta=2/q-5$	$\beta=2\cdot 13/4-5=3/2$
		$p=2\,(1-2q)$	$p=2\,(1-2\cdot 4/13)=10/13$

TABLE 2. Comparison of the scalings for MHD and the Hall cascade.

4. Conclusion

The present work has highlighted the power of dimensional arguments, which were here applied to the case of the Hall cascade without helicity, where the magnetic field is naturally represented as a quantity with units of a magnetic diffusivity. The magnetic helicity density has units of $\mathrm{m}^5\,\mathrm{s}^{-2}$ and the Hosking integral has units of $\mathrm{m}^{13}\,\mathrm{s}^{-4}$, which yields $q=4/13$, $\beta=3/2$, and $p=10/13$. Comparing with standard MHD, where the magnetic field has units of $\mathrm{m\,s}^{-1}$, our exponents p and q are now smaller, but β is still the same in both cases; see Table 2 for a comparison between Hall cascade and MHD. The empirically determined value of β is somewhat larger, but this can be explained by finite scale separation and small Lundquist numbers.

The decay properties of the Hall cascade are important in understanding resistive heating in neutron stars while producing at the same time larger scale magnetic fields at a certain speed through inverse cascading (B20). Such simulations have already been done in spherical geometry (Gourgouliatos *et al.* 2020), but the magnetic field in those simulations did not yet exhibit clear forward or inverse cascading. This is presumably due to their initial magnetic field being strongly localized at intermediate length scales. Using an initial broken power law, as done here, would help producing the expected forward or inverse cascadings, but this may also require much larger resolution than what is currently possible. Similarly, of course, the values of n_e and η are depth dependent in real neutron stars, but the work of B20 showed that this did not affect the scaling behavior of the magnetic decay. Therefore, the importance of the Hosking integral may well carry over to real neutron stars.

The possible role of reconnection in the Hall cascade remains still an open question. In the case of MHD, reconnection has been discussed extensively by Hosking & Schekochihin (2021), making reference to earlier work by Zhou *et al.* (2019, 2020) and Bhat *et al.* (2021). Also in the Hall cascade there is the possibility that the decay of $\mathcal{E}$ could be slowed down in an intermediate range of values of the Lundquist number. As shown in Zhou *et al.* (2022), this could lead to a termination line in the pq diagrams that is different from the $p=2(1-2q)$ self-similarity line discussed here. At the moment, however, there is no compulsory evidence for deviations of the solutions from the self-similarity line.

Acknowledgements

I would like to thank the Isaac Newton Institute for Mathematical Sciences, Cambridge, for support and hospitality during the programme "Frontiers in dynamo theory: from the Earth to the stars" where the work on this paper was undertaken. I am also grateful to the two referees for their comments, which have led to improvements in the presentation.

Funding

This work was supported by EPSRC grant no EP/R014604/1 and the Swedish Research Council (Vetenskapsrådet, 2019-04234). Nordita is sponsored by Nordforsk. We acknowledge the allocation of computing resources provided by the Swedish National Allocations Committee at the Center for Parallel Computers at the Royal Institute of Technology in Stockholm and Linköping.

Declaration of Interests

The authors report no conflict of interest.

Data availability statement

The data that support the findings of this study are openly available on Zenodo at doi:10.5281/zenodo.7357799 (v2022.11.24). All calculations have been performed with the Pencil Code (Pencil Code Collaboration *et al.* 2021); DOI:10.5281/zenodo.3961647.

Author ORCID

A. Brandenburg, https://orcid.org/0000-0002-7304-021X

REFERENCES

Anzuini, F., Melatos, A., Dehman, C., Viganò, D. & Pons, J. A. 2022 Thermal luminosity degeneracy of magnetized neutron stars with and without hyperon cores. *Mon. Not. R. Astron. Soc.* **515** (2), 3014–3027, arXiv: 2205.14793.

Bhat, Pallavi, Zhou, Muni & Loureiro, Nuno F. 2021 Inverse energy transfer in decaying, three-dimensional, non-helical magnetic turbulence due to magnetic reconnection. *Mon. Not. R. Astron. Soc.* **501** (2), 3074–3087, arXiv: 2007.07325.

Biskamp, D., Schwarz, E. & Drake, J. F. 1996 Two-Dimensional Electron Magnetohydrodynamic Turbulence. *Phys. Rev. Lett.* **76** (8), 1264–1267.

Brandenburg, Axel 2020 Hall Cascade with Fractional Magnetic Helicity in Neutron Star Crusts. *Astrophys. J.* **901** (1), 18, arXiv: 2006.12984.

Brandenburg, Axel & Kahniashvili, Tina 2017 Classes of Hydrodynamic and Magnetohydrodynamic Turbulent Decay. *Phys. Rev. Lett.* **118** (5), 055102, arXiv: 1607.01360.

Brandenburg, Axel, Kahniashvili, Tina & Tevzadze, Alexander G. 2015 Nonhelical Inverse Transfer of a Decaying Turbulent Magnetic Field. *Phys. Rev. Lett.* **114** (7), 075001, arXiv: 1404.2238.

Cho, Jungyeon & Lazarian, A. 2009 Simulations of Electron Magnetohydrodynamic Turbulence. *Astrophys. J.* **701** (1), 236–252, arXiv: 0904.0661.

Goldreich, Peter & Reisenegger, Andreas 1992 Magnetic Field Decay in Isolated Neutron Stars. *Astrophys. J.* **395**, 250.

Gourgouliatos, Konstantinos N. & Hollerbach, Rainer 2018 Magnetic Axis Drift and Magnetic Spot Formation in Neutron Stars with Toroidal Fields. *Astrophys. J.* **852** (1), 21, arXiv: 1710.01338.

Gourgouliatos, Konstantinos N., Hollerbach, Rainer & Archibald, Robert F. 2018 Modelling neutron star magnetic fields. *Astron. Geophys.* **59** (5), 5.37–5.42.

Gourgouliatos, Konstantinos N., Hollerbach, Rainer & Igoshev, Andrei P. 2020 Powering central compact objects with a tangled crustal magnetic field. *Mon. Not. R. Astron. Soc.* **495** (2), 1692–1699, arXiv: 2005.02410.

Gourgouliatos, Konstantinos N., Wood, Toby S. & Hollerbach, Rainer 2016 Magnetic field evolution in magnetar crusts through three-dimensional simulations. *Proc. Nat. Acad. Sci.* **113** (15), 3944–3949, arXiv: 1604.01399.

Hosking, David N. & Schekochihin, Alexander A. 2021 Reconnection-Controlled Decay of Magnetohydrodynamic Turbulence and the Role of Invariants. *Phys. Rev. X* **11** (4), 041005, arXiv: 2012.01393.

Hosking, David N. & Schekochihin, Alexander A. 2022 Cosmic-void observations reconciled with primordial magnetogenesis , arXiv: 2203.03573.

Igoshev, Andrei P., Popov, Sergei B. & Hollerbach, Rainer 2021 Evolution of Neutron Star Magnetic Fields. *Universe* **7** (9), 351, arXiv: 2109.05584.

Pencil Code Collaboration, Brandenburg, Axel, Johansen, Anders, Bourdin, Philippe, Dobler, Wolfgang, Lyra, Wladimir, Rheinhardt, Matthias, Bingert, Sven, Haugen, Nils, Mee, Antony, Gent, Frederick, Babkovskaia, Natalia, Yang, Chao-Chin, Heinemann, Tobias, Dintrans, Boris, Mitra, Dhrubaditya, Candelaresi, Simon, Warnecke, Jörn, Käpylä, Petri, Schreiber, Andreas, Chatterjee, Piyali, Käpylä, Maarit, Li, Xiang-Yu, Krüger, Jonas, Aarnes, Jørgen, Sarson, Graeme, Oishi, Jeffrey, Schober, Jennifer, Plasson, Raphaël, Sandin, Christer, Karchniwy, Ewa, Rodrigues, Luiz, Hubbard, Alexander, Guerrero, Gustavo, Snodin, Andrew, Losada, Illa, Pekkilä, Johannes & Qian, Chengeng 2021 The Pencil Code, a modular MPI code for partial differential equations and particles: multipurpose and multiuser-maintained. *J. Open Source Softw.* **6** (58), 2807, arXiv: 2009.08231.

Zhou, Hongzhe, Sharma, Ramkishor & Brandenburg, Axel 2022 Scaling of the Hosking integral in decaying magnetically dominated turbulence. *J. Plasma Phys.* **88** (6), 905880602, arXiv: 2206.07513.

Zhou, Muni, Bhat, Pallavi, Loureiro, Nuno F. & Uzdensky, Dmitri A. 2019 Magnetic island merger as a mechanism for inverse magnetic energy transfer. *Phys. Rev. Res.* **1** (1), 012004, arXiv: 1901.02448.

Zhou, Muni, Loureiro, Nuno F. & Uzdensky, Dmitri A. 2020 Multi-scale dynamics of magnetic flux tubes and inverse magnetic energy transfer. *J. Plasma Phys.* **86** (4), 535860401, arXiv: 2001.07291.